ACS APPLIED MATERIALS & INTERFACES

Research Article

www.acsami.org

Graphene-Coated Surface Plasmon Resonance Interfaces for Studying the Interactions between Bacteria and Surfaces

Palaniappan Subramanian,[†] Fatiha Barka-Bouaifel,[†,‡] Julie Bouckaert,[*,§] Nao Yamakawa,[§] Rabah Boukherroub,[†] and Sabine Szunerits[*,†]

[†]Institut de Recherche Interdisciplinaire (IRI), CNRS USR 3078, Université Lille1, Parc de la Haute Borne, 50 avenue de Halley, BP 70478, 59658 Villeneuve d'Ascq, France

[‡]Laboratoire de Technologie des Matériaux et de Génie des Procédés (LTMGP), Université Abderrahmane Mira de Béjaia, Targa Ouzemour, 06000 Béjaia, Algérie

[§]Unité de Glycobiologie Structurale et Fonctionnelle (UGSF), Université Lille1, CNRS UMR 8576, 59655 Villeneuve d'Ascq, France

ABSTRACT: A variety of physical and chemical parameters are of importance for adhesion of bacteria to surfaces. In the colonization of mammalian organisms for example, bacterial fimbriae and their adhesins not only seek particular glycan sequences exposed on diverse epithelial linings, they also enable the bacteria to overcome electrostatic repulsion exerted by their selected surfaces. In this work, we present a new technique based on simplified model systems for studying the adhesion strength of different *Escherichia coli* strains. For this purpose, gold-based surface plasmon resonance (SPR) interfaces were coated with thin films of reduced graphene oxide (rGO) through electrophoretic deposition. The rGO matrix was post-modified with polyethyleneimine (PEI), poly(sodium 4-styrenesulfonate) (PSS), mannose, and lactose through π-stacking and/or electrostatic interactions by simple immersion of the SPR interface into their respective aqueous solutions. The adhesion behaviors of one uropathogenic and two enterotoxigenic *Escherichia coli* clinical isolates, that each express structurally characterized fimbrial adhesins, were investigated. It was found that the UTI89 cystitis isolate that carries the mannose-binding FimH adhesin was most attracted to the PEI- and mannose-modified surfaces, whereas the att25 diarrhoeal strain with the *N*-acetylglucosamine-specific F17a-G adhesin disintegrated the lactose-modified rGO. The highly virulent 107/86 strain interacted strongly with the PSS-modified graphene oxide, in agreement with the polybasic surroundings of the ABH blood group-binding site of the FedF adhesin, and showed a linear SPR response in a concentration range between 1×10^2 and 1×10^9 cfu/mL.

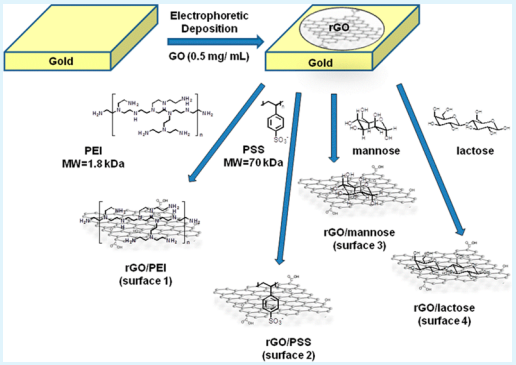

KEYWORDS: *Escherichia coli, reduced graphene oxide, polyethyleneimine (PEI), mannose, lactose, poly(sodium-4-styrenesulfonate (PSS), surface plasmon resonance*

1. INTRODUCTION

The *Escherichia coli* (*E. coli*) bacterium has been intensively investigated over the last decades and is the most widely studied prokaryotic model organism for its importance in the field of biotechnology and microbiology. Enterohaemorrhagic *E. coli* (EHEC) has been recognized as being the cause of serious illness and mortality in outbreaks of foodborne illness.[1] *E. coli* O157:H7 is one of the pathogenic bacteria of most concern, but the problem is at large as other pathogenic *E. coli* strains are known to cause foodborne and waterborne illnesses. The sensitive detection as well as the discrimination of different *E. coli* strains remains thus of uttermost importance. Pathogenic *E. coli* bacteria possess one or more virulence factors that determine the microbial pathogenicity and increase the fitness of a pathogen during infection.[2−4] A well-known virulence factor in uropathogenic *E. coli* (UPEC) is FimH, a mannose-binding adhesin found at the tip of the type 1 pilus produced by most of the enterobacteriaceae family, including UPEC.[4−6] It was found that most FimH variants from uropathogenic, faecal and enterohaemorrhagic isolates express the same specificity and affinity to mannose structures,[6] with the only exception being a FimH from *E. coli* O157:H7 strains.[7] The effect of FimH variation and mutation on bacterial adherence has mainly evaluated by means of the hemagglutination assay, yeast agglutination assay, and by analysis of the adherence and invasion into bladder epithelial cells.[3,8−10]

Competition binding experiments on SPR interfaces modified with Fab fragments of the monoclonal antibody 1C10, recognizing mannose-binding sites of FimH, have in addition been used to determine the solution affinity of FimH-carbohydrate interactions.[4,6,9] Other available quantitative methods are based on culture and colony counting methods,

Received: October 3, 2013
Accepted: January 16, 2014
Published: January 16, 2014

   dx.doi.org/10.1021/am405541z | ACS Appl. Mater. Interfaces 2014, 6, 5422−5431

polymerase chain reaction (PCR), enzyme-linked immunosorbent assay (ELISA), or on a DNA-based nanobarcode detection strategy.[11−13] While the latter two methods have proven to be fast and sensitive, they require pretreatment and cell lysis to extract DNA. Strategies based on the direct detection of the whole microorganism using SPR[11−16] or electrical impedance spectroscopy (EIS)[12,13,16,17] have shown to give reliable results in much shorter time and have consequently drawn a lot of interest. The required selectivity is achieved using surface-immobilized polyclonal antibodies,[16,18,19] lectins,[20] and carbohydrates such as α-D-mannoside,[12] antimicrobial peptides,[15,21] or bacteriophages.[22,23]

In recent years, graphene and its derivatives, graphene oxide (GO) and reduced graphene oxide (rGO), have been investigated for their efficiency in pathogen capture, detection, and killing.[24,25] The usability of these 2D nanomaterials results from their heterogeneous plane structures featuring ionic and aromatic components that facilitate chemical bonding and noncovalent interactions (π−π stacking, electrostatic, H-bonding, etc.) with a variety of molecules.[26] We have shown that graphene-coated SPR interfaces have several advantages over gold-based SPR interfaces.[27,28] The high surface-to-volume ratio of graphene[27,29] and rGO[28] has proven to be beneficial for efficient adsorption of biomolecules when compared to naked gold due to possible π-stacking interactions between the carbon-based ring structures of biological molecules and the hexagonal cells of graphene.[28,30]

The motivation of the present study is to use graphene-based SPR chips as novel interfaces to investigate in a facilitated manner the interaction preference and strength of *E. coli*. pathogens. In a proof of principle that such simplified model interfaces can provide some answers to fundamental questions concerning cell adhesion, positively, negatively. and glycan-modified SPR interfaces were fabricated. Positively charged SPR interfaces were formed by modification of the graphene-based SPR interface with polyethyleneimine (PEI). The integration of poly(sodium 4-styrenesulfonate) (PSS) resulted in a strongly negatively charged interface. The concept of the surface modification is based on π−π stacking interaction between the aromatic structures of the polymers and the graphene matrix. This approach prevents the need of pre-functionalization of the polymers by thiol and other functional linkers and makes the concept of interest for the integration of many other organic molecules. In the case of PEI and PSS modifications, different electrostatic interactions with the graphene interface are expected to be essentially responsible for discrimination between *E. coli* strains. On the other hand, glycan-modified interfaces should be able to distinguish bacteria specific for simple monosaccharides, such as the mannose-binding UTI89 strain and the *N*-acetylglucosamine-binding att25 strain. It has been verified that the binding UTI89 *E. coli* to the mannose-modified interface was mannose-specific binding, using a mutation in the mannose-binding pocket (UTI89 Q133K)[3] and using a *fimH* knock-out (UTI89 *fimH*$^-$), in the otherwise isogenic UTI89 strain (Table 2).[8] The potential of the interfaces for analytical purposes was also investigated. *E. coli* 107/86 is known to cause oedema disease in pigs at the age of weaning. It produces a Shiga toxin II variant in the digestive tract that is absorbed into the circulation and that causes lesions in the vasculature of the intestine, subcutis, and brain.[31] Quantitative and qualitative information on the presence of *E. coli* strain 107/86 is thus of interest.

2. EXPERIMENTAL SECTION

2.1. Materials. Graphite powder (<20 micrometers), hydrogen peroxide (H_2O_2), sulfuric acid (H_2SO_4), dimethylsulfoxide (DMSO), mannose, lactose, polyethyleneimine (PEI) (MW = 1.8 kDa), and poly(sodium 4-styrenesulfonate) (PSS) (MW = 70 kDa), were purchased from Aldrich and used as received.

2.2. Formation of rGO-SPR Interfaces. Graphene oxide (GO) was synthesized from graphite powder by a modified Hummers' method[32] for which the detailed experimental conditions are reported.[33] GO was exfoliated in milli-Q water (0.5 mg/mL) by ultrasonication for 3 h until the solution became clear with no visible particulate matter.

Gold-based SPR interfaces were formed by depositing 5 nm of titanium and 50 nm of gold successively onto cleaned glass slides by thermal evaporation.

The electrophoretic deposition was carried out using a two-electrode cell containing the GO aqueous dispersion (0.5 mg/mL) by applying DC voltage (150 V) for 20 s. Platinum (Pt) foil (1 × 2 cm^2) acts as the cathode and the SPR interface [glass/Ti (5 nm)/Au (50 nm)] substrate as the anode. The two electrodes were separated by 1 cm and were placed parallel to each other in the GO dispersion. After deposition, the rGO-SPR interface was washed with deionized water (three times) followed by blow drying with nitrogen.

2.3. Functionalization of the rGO-SPR Interfaces. The rGO-SPR interfaces and gold-based interfaces were immersed for 2 h in 100 mM aqueous solutions of PEI, PSS, mannose or lactose before being rinsed three times with water. Diluted rGO/PEI interfaces were formed by their immersion into 10 mM, 1 mM and 0.1 mM PEI solutions for different time intervals.

2.4. Determination of the Amount of Mannose (lactose) on Mannose (lactose)/Au/rGO-Modified Interfaces. The amount of glycan was determined by treatment with a phenol/H_2SO_4 solution as described previously.[7] First, a calibration curve for mannose or lactose in solution was established using a phenolic aqueous solution (5 wt %, 60 μL), concentrated H_2SO_4 (900 μL), which was added to an aqueous mannose solution (60 μL) and stirred for 10 min, and then an absorption spectrum was recorded (Perkin Elmer Lambda 950 dual beam) against a blank sample (without glycan). The absorbance of the solution was measured at two wavelengths, λ_1 = 485 and λ_2 = 570 nm, and the absorbance difference ($A_{485} - A_{570}$) was plotted against the concentration of the glycan. The glycan-modified Au/rGO SPR interface was treated with phenol/H_2SO_4 following the same protocol as described above.

2.5. Bacterial Strains. The *E. coli* strains have been cultured on LB-agar complemented with the appropriate antibiotics for the engineered strains. Upon overnight growth at 37 °C, colonies were harvested by scraping them off the agar and diluted in phosphate-buffered saline to different concentrations. Bacterial concentrations were determined by measuring the optical density at 600 nm using a Perkin Elmer Lambda UV/Vis 950 spectrophotometer and a conversion of $OD_{600\ nm}$ with 0.66 = 1 × 10^9 cfu/mL.

2.6. Instrumentation. *2.6.1. X-ray Photoelectron Spectroscopy (XPS).* X-ray photoelectron spectroscopy (XPS) measurements were performed with an ESCALAB 220 XL spectrometer from Vacuum Generators featuring a monochromatic Al K_α X-ray source (1486.6 eV) and a spherical energy analyzer operated in the CAE (constant analyzer energy) mode (CAE = 100 eV for survey spectra and CAE = 40 eV for high-resolution spectra), using the electromagnetic lens mode. The detection angle of the photoelectrons is 30°, as referenced to the sample surface. After subtraction of the Shirley-type background, the core-level spectra were decomposed into their components with mixed Gaussian-Lorentzian (30:70) shape lines using the CasaXPS software. Quantification calculations were performed using sensitivity factors supplied by PHI.

2.6.2. SPR Instrumentation. The surface plasmon resonance instrument used was an Autolab ESPRIT instrument (Eco Chemie, Utrecht, The Netherlands) with an incident laser light with 670 nm wavelength. The configuration of this equipment is described elsewhere.[34,35] The instrument is equipped with a cuvette of about 100 μL. The prism used had a refractive index of *n* = 1.52. WinSpall

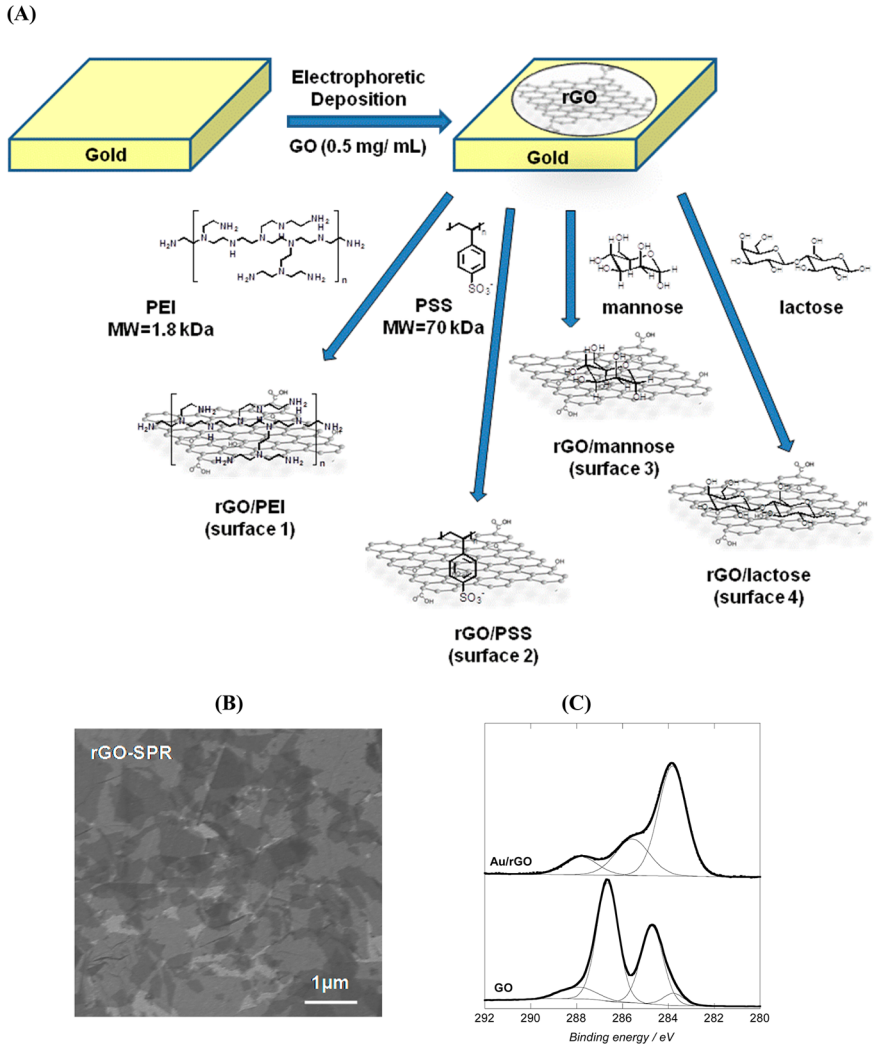

Figure 1. (A) Schematic illustration of the different SPR interfaces investigated; (B) SEM image of the gold-based SPR interface coated with reduced graphene oxide through electrophoretic deposition of GO; (C) C1s core-level XPS spectra of initial GO and of a Au/rGO-SPR interface.

Table 1. Physicochemical Properties of rGO-Modified SPR Interfaces

		surface rGO	surface 1 rGO/PEI	surface 2 rGO/PSS	surface 3 rGO/mannose	surface 4 rGO/lactose
XPS	C1s (at. %)	77.3	64.9	68.6	56.7	57.3
	O1s (at. %)	22.7	24.7	29.1	43.3	42.7
	other (at. %)		10.4 (N1s)	2.3 (S2p)		
water contact angle (deg)		58 ± 1	80 ± 1	70 ± 1	15 ± 3	12 ± 3
zeta potential of matrix (mV)		−32 ± 3	+52 ± 2	−57 ± 2	−39 ± 2	−38 ± 2

2.0 software (Max-Planck-Institute for Polymer Research, Mainz) was used to calculate the SPR curves and approximate the experimental dependences with an optical model within the framework of Maxwell macroscopic approach. The data recorded in this manuscript were collected from five different experiments.

2.6.3. Zeta-Potential Measurements. Zeta-potential measurements were performed on electrophoretically deposited Au/rGO and functionalized Au/rGO matrices after the dissolution of the matrix from the Au interface in DMSO and resuspension into water using a Zetasizer Nano ZS (Malvern Instruments S.A., Worcestershire, U.K.) using the electrophoretic mode.

2.6.4. Confocal Microscope Images. Confocal images were acquired with a 60× objective (Nikon Plan Apo VC, NA=1.2 on a Nikon A1R confocal microscope, Nikon Biosceince, Confocal Systems, Nikon ECLIPSE FN1 fixed stage France) equipped with a 488 nm excitation argon laser and an Eclipse FN1 fixes stage direct microscope. The SIMPLEPCI software (Comprox Imaging Systems, Cranberry Township, PA) was used for image capture. Photomultiplier tube back levels were kept as a default of 600 for transmitted light images.

3. RESULTS AND DISCUSSION

3.1. Preparation Modified Reduced Graphene Oxide-Coated SPR Interfaces (rGO-SPR). The rGO-SPR interface was prepared as described previously (Figure 1A).[28] The process consists of the electrophoretic depositon of rGO onto gold-SPR interface through the application of a voltage of 150 V for 20 s. The GO platelets with a zeta-potential of −35 mV migrate towards the positively biased gold-based SPR interface, when a DC voltage is applied.

Figure 1B displays a scanning electron microscopy (SEM) image of the Au/rGO SPR interface. It shows that the rGO film

dx.doi.org/10.1021/am405541z | ACS Appl. Mater. Interfaces 2014, 6, 5422−5431

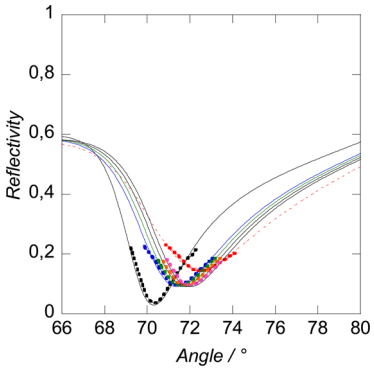

Figure 2. SPR curves of the sensor before (black), after electrophoretic modification with rGO forming Au/rGO (blue), and post-treatment of Au/rGO with mannose (green), lactose (orange), PEI (violet), and PSS (red); electrophoretic deposition time, 20 s; DC voltage, 150 V. The dotted lines are the experimental data and the solid lines are SPR fits: [n_{prism}= 1.52, n_{Ti} = 2.36 + *i*3.47 (*d* = 5 nm); n_{Au} = 0.197 + *i*3.67 (*d* = 50 nm); $n_{graphene}$ = 3.0 + *i*1.216; *n*(PSS) = 1.45; λ = 670 nm].

is homogenously deposited over the gold surface. The C1s core level XPS spectrum of the Au/rGO SPR interface (Figure 1C) indicates clearly that GO was reduced to rGO during the electrophoretic deposition. The XPS spectrum can be deconvoluted into three dominant bands at 283.8 (sp^2-hybridized carbon), 285.5 (C−OH), and 287.3 eV (C═O) with a C/O ratio of 3.3 (Table 1). This is different to the initial GO oxide solution where the C1s core level XPS spectrum displayed contributions at 283.8, 284.7, 286.7, and 287.9 eV assigned to sp^2-hybridized carbon, C−H/C−C, C−O, and C═O species, respectively, with a C/O ratio of 1.73.[28]

The SPR signal of the Au/rGO SPR interface is depicted in Figure 2. From the SPR angle shift of the Au/rGO SPR interface, the thickness of the electrophoretically deposited rGO can be estimated to be approximately 2 nm, corresponding to about 5−6 graphene layers.[36] Such interfaces were in the following modified with polyethyleneimine (PEI, 1.8 KDa), poly(sodium 4-styrenesulfonate) (PSS, 70 KDa), D-mannose, or D-lactose (Figure 1A). Stable interfaces were formed by incubating the Au/rGO SPR interfaces for 2 h in the aqueous solution (100 mM) of the reactant. The molecular adsorption onto rGO occurs through π-stacking and/or electrostatic interactions, resulting in stable SPR interfaces. The sucessful integration of the different molecules onto Au/rGO and information on the chemical composition of the modified interfaces were obtained by XPS analysis (Table 1). In the case of Au/rGO/PEI, besides C1s and O1s contributions N1s with an atomic percentage of 10.3% was found. The integration of PSS onto Au/rGO is evidenced by the presence of S2p (2.3 at %) (Table 1).

The amounts of mannose and lactose loaded onto Au/rGO SPR were determined using a colorimetric assay, based on the specfic reaction of carbohydrates with phenol in concentrated sulfuric acid as previously described.[37] The method allowed the amount of sugar to be estimated as $\Gamma_{mannose}$ = (5.8 ± 0.6) × 10^{12} molecules cm^{-2} and $\Gamma_{lactose}$ = (3.4 ± 0.6) × 10^{12} molecules cm^{-2}. These interfaces were in the following used for carbohydrate-specific detection of the different *E. coli* strains.

3.2. Adhesion Behavior of Different *E. coli* Strains on Au/rGO SPR Interfaces. As charge is known to play an important role in bacterial adhesion, the interactions of five *E. coli* strains with rGO matrices with a zeta potential of ζ = +52 ± 2 mV and ζ = −57 ± 2 mV (Table 1), formed through interaction with polyethyleneimine (PEI) and poly(sodium 4-styrenesulfonate) (PSS), respectively, were investigated using

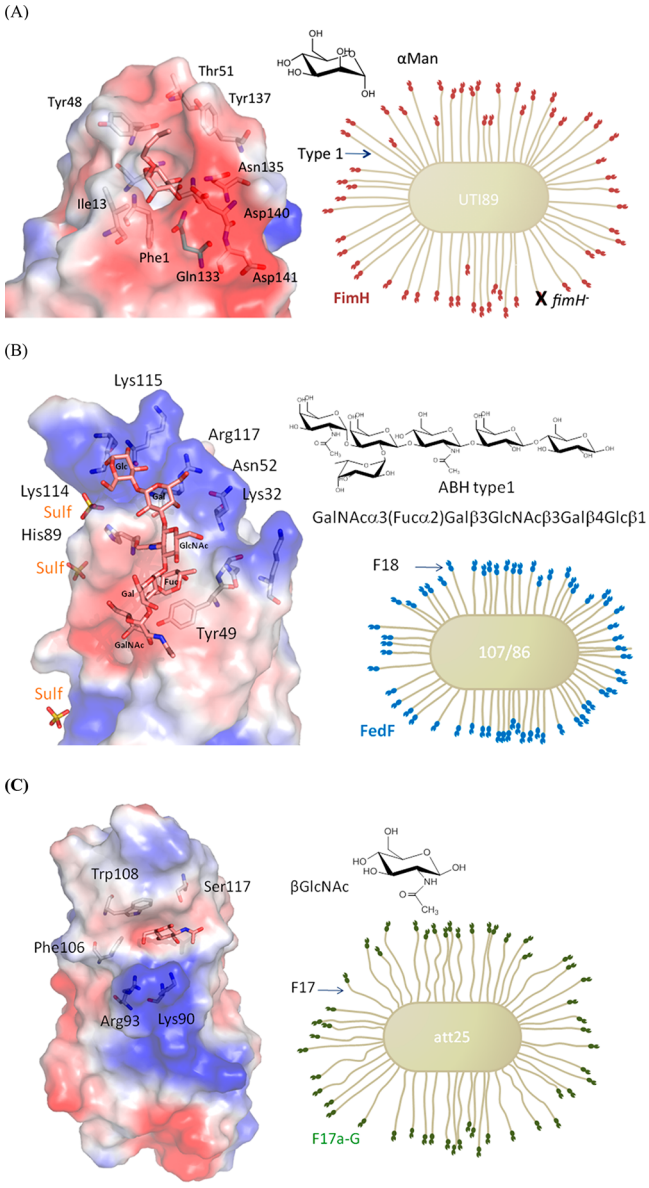

Figure 3. Schematic illustration of charge distribution on the different *E. coli* strains. (A) UTI89 Electrostatic surface of the mannose-binding site is depicted in blue (for positive charge and for nitrogen atoms) and red (for negative charge and for oxygen atoms) for the FimH-butyl α-D-mannose complex. (PDB entry 1TR7, that has an open gate (Tyr48-Tyr137) conformation where the butyl chain travels through). Gln133 is indicated in cyan; this is an amino acid crucial for mannose binding and was mutated to lysine in the Q133K strain. Amino acid ligands for the butyl α-D-mannose and residues contributing to the negatively charged binding site of FimH are shown in ball-and-stick model. (B) View on the electrostatic surface of the FedF lectin domain where it makes a complex with blood group A type 1 hexasaccharide (PDB entry 4B4Q). The tip of FedF near the binding site is highly seeded with positive charges (blue) from lysine and arginine residues. The fucose is in π-stacking with Tyr49. Bound sulfate ions (sulfur in yellow) are shown (PDB entry 4BWO). (C) F17a-G in complex with *N*-acetylglucosamine (PDB entry 1O9W) is polar to electronegative (red) in charge in the binding site, compensated by a positively charged patch (blue) underneath for which no ligand is currently known. Aromatic π-stacking happens with Trp108.

dx.doi.org/10.1021/am405541z | ACS Appl. Mater. Interfaces 2014, 6, 5422−5431

Table 2. Pathogenicity and Characteristics of the Five Different *E. coli* Strains Investigated

E. coli strains	pathogenicity of *E. coli* strains	characteristics of the fimbriae and fimbrial adhesins	zeta potential (mV)
UTI89	isolate from patient with an acute bladder infection	type-1 fimbriae with mannose-binding FimH adhesin	−35 ± 2
107/86	causes oedema disease in just-weaned piglets	F18 fimbriae with the FedF adhesin as the colonization factor: basic residues juxtaposed to the binding site	−24 ± 2
att25	Bovine isolate of enterotoxigenic, diarrhoeal *E. coli*	F17 fimbriae with *N*-acetylglucosamine-specific adhesin	−30 ± 2
UTI89 *fimH*$^-$	isogenic to UTI89 apart from deletion of *fimH*	no adhesion, thus abrogating mannose binding	−36 ± 2
UTI89 Q133K	UTI89 with Gln133 to Lys mutation in the binding pocket of FimH, thus abrogating mannose binding		−35 ± 2

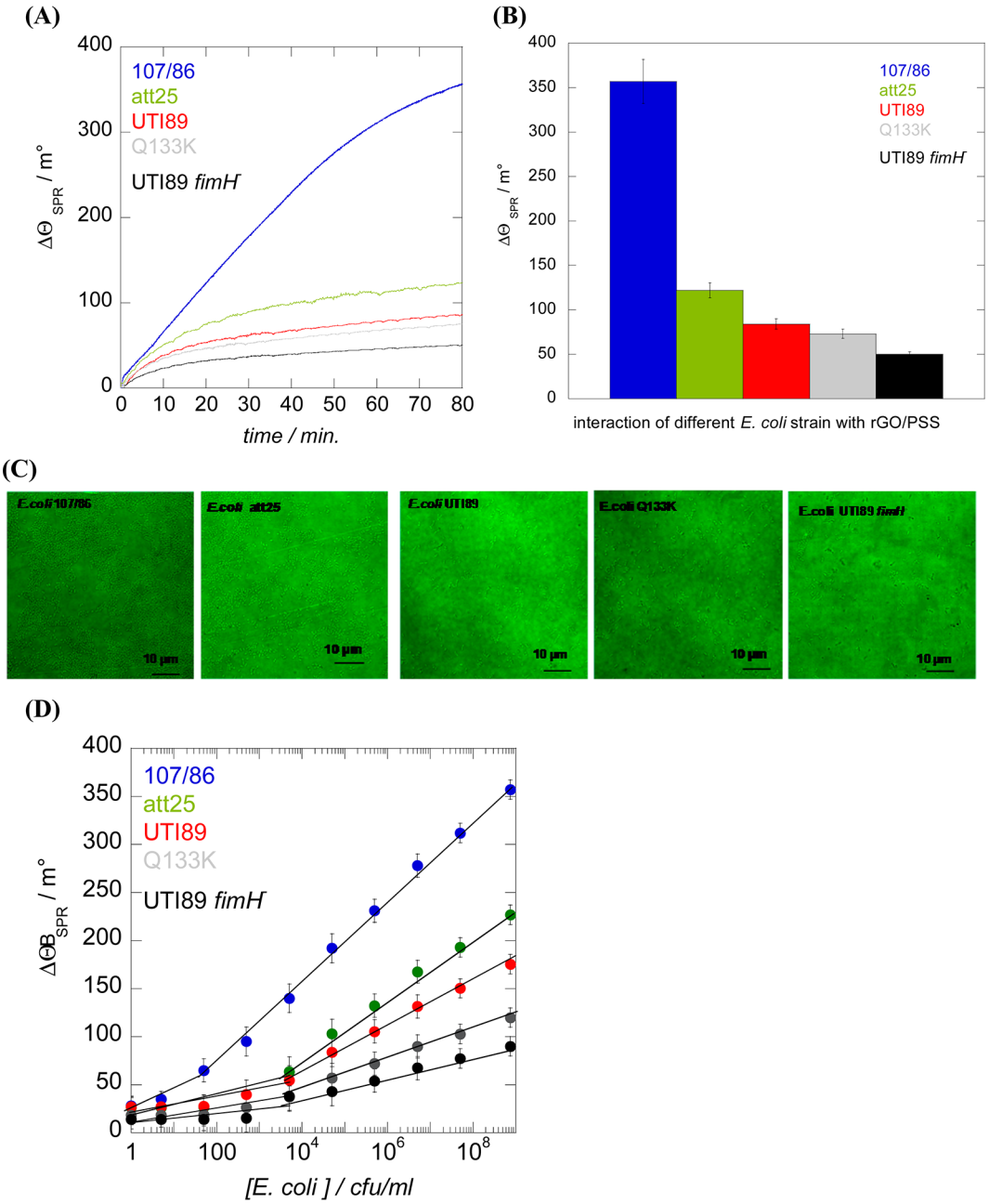

Figure 4. (A) SPR responses recorded on Au/rGO/PSS upon addition of different *E. coli* strains (c = 1.5 × 10^9 cfu/mL): 107/86 (blue), att25 (green), UTI89 (red), UTI89 Q133K (grey), UTI89 *fimH*$^-$ (black). (B) Bar diagram of SPR responses on Au/rGO/PSS after 80 min for different *E. coli* strains. (C) Confocal images of different bacteria strains (bright rod-shaped spots) on Au/rGO/PSS. (D) Calibration curve on Au/rGO/PSS SPR interfaces for different concentrations of the different *E. coli* strains.

dx.doi.org/10.1021/am405541z | *ACS Appl. Mater. Interfaces* 2014, 6, 5422−5431

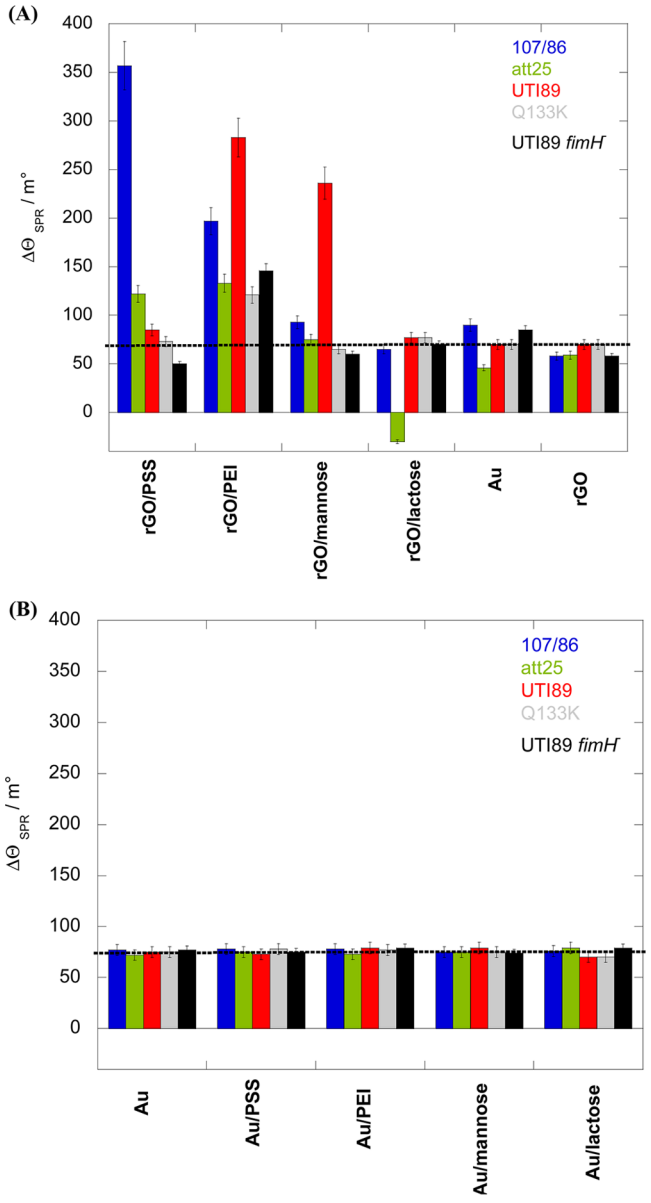

Figure 5. Bar diagramm summarizing all the recorded changes of the SPR response upon addition of 1.5×10^9 cfu/mL *E. coli* strains onto differently modified (A) rGO and (B) gold interfaces. Five replicate measurements were performed for each experiment: 107/86 (blue), att25 (green), UTI89 (red), UTI89 Q133K (grey), UTI89 *fimH*$^-$ (black).

SPR. The integration of PEI with a low molecular weight of 1.8 kDa did not alter significantly the SPR signal, whereas integration of the high molecular weight (MW = 70 KDa) PSS resulted in a red shift as seen in Figure 2.

We used in this study one uropathogenic (UTI89) and two enterotoxigenic *E. coli* (107/86 and att25) clinical isolates, that each expresses structurally characterized fimbrial adhesins (Figure 3). Differentiation of *E. coli* strains is known to evolve due to the presence of virulence factors, such as the FimH adhesin, that when lost or mutated result in an altered capability of colonization and avidity to cell surfaces and surfaces in general.[4] This "biochemical" perception of bacterial interaction with surfaces is additionally originating from an interplay between attractive and repulsive electrostatic forces, hydrogen bonding and other physico-chemical parameters such as hydrophobicity, surface roughness, etc.[38,39,42] Figure 3 shows the distribution of positively (blue color) and negatively (red color) charges present at the very end of the fimbriae of each of the pathogens. The amino acid ligands for the butyl α-D-mannose and residues contributing to the binding site of FimH are in addition shown in the ball and-stick model. From this illustration it becomes obvious that UTI89 presents a strongly localized negative charged mannose- binding pocket, whereas 107/89 shows an accumulation of positive charge bordering the blood group sugar binding groove at the tip of FedF lectin domain. The F17a-G lectin domain in complex with N-acetylglucosamine, of the *E. coli* att25 strain, is polar to electronegative in charge in the binding site, but this is neutralised by a positively charged handle underneath the monosaccharide-binding site. The adhesion of two control *E. coli* strains was investigated. The UTI89 Q133K and UTI89 *fimH*$^-$ strains serve as negative controls for the otherwise isogenic UTI89 *E. coli* strain (Table 2). Table 2 shows in addition the experimentally measured zeta potential of the whole *E. coli* cell. Although there are local charge changes around the binding site of the lectin domain of the adhesin (Figure 3), the global charge of the bacteria is always negative.

SPR studies were carried out to measure the bacterial capture activity of the functionalized SPR interfaces. Figure 4A shows the change of the SPR angle over time upon addition of *E. coli* strains (1.5×10^9 cfu/mL) onto negatively charged PSS-coated rGO interfaces. A significantly different adhesion behavior was observed for *E. coli* 107/86, with a three times higher shift in SPR angle compared to the other *E. coli* strains (Figure 4B). As shown in Figure 3B, the F18 fimbriae of *E.coli* 107/86 carries the FedF adhesin that is positively charged at the tip. Enhanced electrostatic interaction with the negatively charged PSS matrix and the positive charge at the tip of the FedF adhesin[4] of *E. coli* stain 107/86 is most likely at the origin for enhanced affinity and thus larger capture density (Figure 4A). A somewhat larger capture activity was also observed with *E.coli* att25, specific strain presenting some positive charges underneath the *N*-acetylglucosamine-binding pocket as illustrated in Figure 3C (Lys90, Arg93). The increased change in SPR angle correlates to increased baterial adhesion, as confirmed by confocal microscopy images (Figure 4C).

In addition to electrostatic interactions, $\pi-\pi$ stacking has also to be considered in this system. However, as seen in Figure 5A summarizing SPR data on the different rGO interfaces for each *E. coli* strain, bacterial adhesion to rGO is independent of the used *E. coli.* being of the same order of magnitute ($\approx$ 80 millidegrees) for all tested strains. Furthermore, the importance of rGO is furthermore evidenced when comparing the adhesion behavior of the different *E. coli* strains to gold interfaces modified in the same way as rGO. As can be decuded from Figure 5B, no differentiation is obverved on such SPR interfaces thus addressing the role of rGO in bacterial adhesion. In addition, bacterial adhesion to rGO is comparable to non-specific adsorption on gold. It can be concluded, that $\pi-\pi$ stacking interactions are minimaly involved in the differential binding of the *E. coli* strains under study. In contrast, the degree of charge seems to be an important parameter defining bacterial adhesion. The experimental data indicate that an SPR interface with a zeta potential of -32 ± 3 mV is not sufficient negatively charged to allow strong electrostatic interactions to take place. Indeed, the zeta potential of rGO is negative as is the case of rGO/PSS, but its absolute value is approximately half that of Au/rGO/PSS (Table 1). The overall zeta potential of the *E. coli*

dx.doi.org/10.1021/am405541z | ACS Appl. Mater. Interfaces 2014, 6, 5422−5431

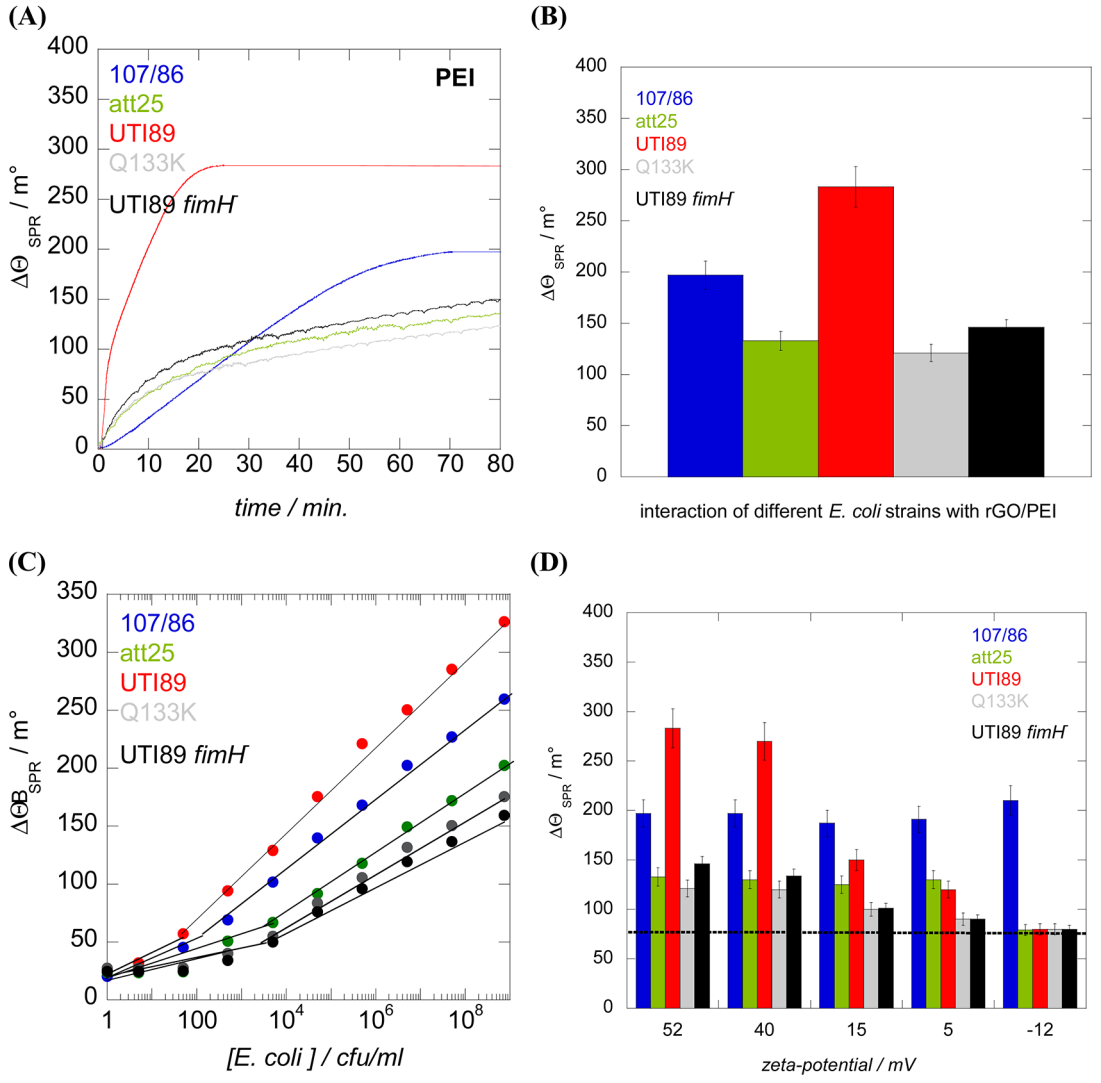

Figure 6. (A) SPR responses recorded on Au/rGO/PEI interfaces upon addition of different *E. coli* strains ($c = 1.5 \times 10^9$ cfu/mL): 107/86 (blue), att25 (green), UTI89 (red), Q133K (grey), UTI89 *fimH*$^-$ (black). (B) Bar diagram of SPR responses on Au/rGO/PEI after 80 min for different *E. coli* strains. (C) Calibration curve on Au/rGO/PEI SPR interfaces for different concentrations of the different *E. coli* strains. (D) Change in SPR responses on Au/rGO/PEI by changing the amount of PEI integrated onto the interface and thus the zeta-potential of the matrix.

strains is negative, the least so far is the 107/85 strain (-24 ± 2 mV) (Table 2) that is the first one to overcome the electrostatic repulsion by specific bacterial adhesion via the FedF adhesin binding pocket.

The SPR results indicate that a PSS-modified Au/rGO SPR interface allows for a partially selective detection of the *E. coli* strain 107/86. As mentioned previously, specific interaction of bacteria with SPR interfaces is currently achieved using monoclonal antibodies,[16,40] protein G,[19,44] and bacteriophages.[22,41,43] Major disadvantages of antibodies are their relative instability, limiting their long-term storage and increasing the production cost. Bacteriophages, viruses recognising and binding specific receptors on host bacteria, are somewhat easier to produce and have a longer storage time, but they suffer from poor surface coverage and subsequent bacterial capture.[23] To determine the sensor sensitivity, the PSS-modified rGO surface was tested with a concentration series of *E. coli* 107/86 (Figure 4D). The SPR angle varies linearly with the 107/86 concentration with a linear response between 1×10^2 and 1×10^9 cfu/mL range and a detection limit of $\approx 10^2$ cfu/mL. In contrast, the detection limits of the other *E. coli* strains were around 10^4 cfu/mL. The detection limit for *E. coli* 107/86 is comparable to other methods used for pathogen analysis based on fluorescence or electrochemical impedance spectroscopy.[17] It is also comparable to bacteriophage-modified SPR chips for detection of O157:H7 *E. coli*,[22] or *E. coli* K-12,[41] but is more sensitive than other SPR-based *E. coli* platforms.[16,19]

Parallel experiments were performed on positively charged Au/rGO/PEI interfaces (Figure 6A). The strongest interaction was observed with UTI89 (Figure 6B) with a detection limit of around 100 cfu/mL (Figure 6C), sufficient for a high positive predictive value for cystitis in symptomatic women.[45] The discrimination of UTI89 from the other *E. coli* strains is less pronounced than was the case for *E. coli* strain 107/86 on Au/rGO/PSS (Figure 4B); however, it is the only *E. coli* strain that stands out, indicating a specific interaction of the UTI89 strains with the PEI-modified interface. This agrees with the local, negative charge accumulation at the lectin domain end of the FimH adhesin at the edge of type-1 fimbriae (Figure 3A). The specificity of the interaction proper to the adhesin was confirmed using two mutations of UTI89: either glutamine 133 to the basic lysine (Q133K, which would render the

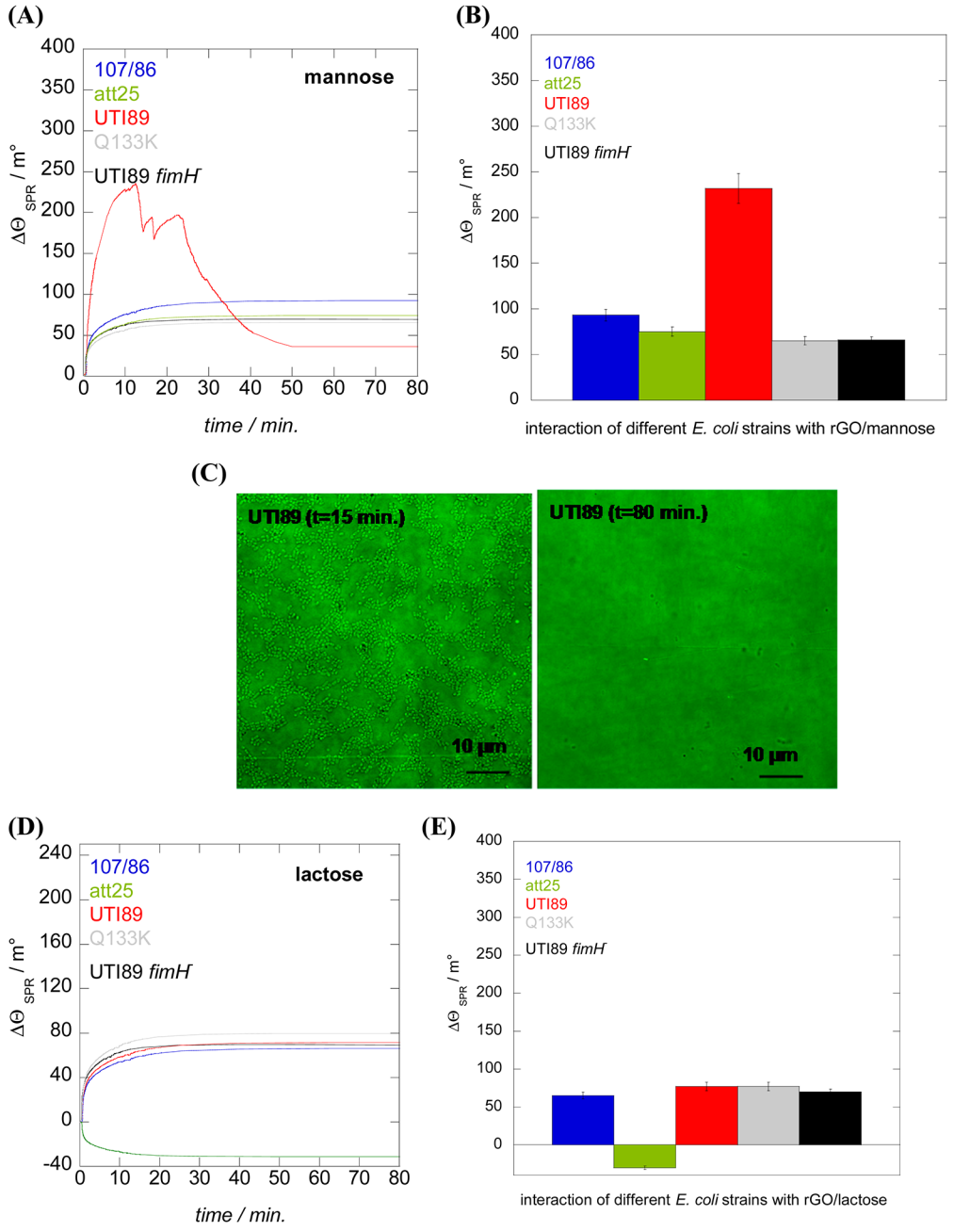

Figure 7. (A) SPR responses recorded on Au/rGO/mannose interfaces upon addition of different *E. coli* strains (c = 1.5 × 10^9 cfu/mL): 107/86 (blue), att25 (green), UTI89 (red), Q133K(grey), UTI89 *fimH*$^-$ (black). (B) Bar diagram of SPR responses on Au/rGO/mannose. (C) Confocal images of *E. coli* strain UTI89 after interaction for 15 min (left) and 80 min (right) on Au/rGO/mannose. (D) SPR responses recorded on Au/rGO/lactose interfaces upon addition of different *E. coli* strains (c = 1.5 × 10^9 cfu/mL): 107/86 (blue), att25 (green), UTI89 (red), UTI89 mut (grey), UTI89 *fimH*$^-$ (black). (E) Bar diagram of SPR responses on Au/rGO/lactose.

binding pocket more positively charged however specific binding is abolished,[7] or by the deletion of the adhesin (UTI89 *fimH*$^-$), that equally nihilates specific binding. Both showing a decreased affinity to rGO/PEI when compared to UTI89, with a difference that corresponds to the difference between UTI89 binding to mannose-modified surface and those of the UTI89 non-binding mutants. Because the Q133K and *fimH*$^-$ mutation and deletion abolish specific recognition by the FimH adhesin, the negative charge localized in the binding site (Figure 3A) only configures a role in the case of fimbrial adhesin-mediated specific bacterial adhesion.

To investigate in more detail the effect of surface charge on the change of bacteria affinity, we formed rGO/PEI interfaces with varying zeta potentials by varying the amount of PEI integrated onto the rGO matrix (Figure 6D). In the case of UTI89, decreasing the zeta potential of the matrix results in a decrease in UTI89 affinity to rGO/PEI. These results support the observation that the specific, adhesion-mediated, bacterial adhesion of UTI89 to rGO/PEI is enhanced by local charges in and around the binding site. There is indeed no significant effect of dilution of PEI on the affinity of *E. coli* strain 107/86. Some binding independent of PEI concentration and thus charge of the surface is observed (Figure 6D). The adhesion of

dx.doi.org/10.1021/am405541z | ACS Appl. Mater. Interfaces 2014, 6, 5422−5431

strains Q133K and UTI89 *fimH*$^-$ to rGO/PEI was also always higher than that on unmodified rGO (−32 mV) (≈80 millidegrees), mannose- (−39 mV) on PSS-modified rGO (−57 mV) (Figure 5A). Considering that the overall charge of each of the *E. coli* strains is negative (Table 2), favoring electrostatic interactions between the *E. coli* and the positively charged interface, this might not seem suprising. The imine-modified Au/rGO/PEI leads to increased background or basal level of bacterial binding and is not likely to be mediated by the fimbrial adhesin. The PEI modification itself seems responsible for some interactions in a charge independent way as the affinity to even slighly negatively charged rGO/PEI (zeta potential =-12 mV) is stronger (Figure 6D) than on negatively charged rGO (Figure 5A). *E. coli* is possibly attracted to a killer surface: the viability of *E. coli* has been reported to decrease dramatically on positively charged, amine-coated surfaces.[39] The increase in basal level of binding moreover differs between the *E. coli* strains, for each of the three *E. coli* strain expresses, besides the fimbrial type, different biopolymers on its surface such as flagellae and lipopolysaccharides. The latter LPS can explicitely carry negatively charged compounds, such as kdo, which is a bacterial variant of sialic acid. The basal level of binding, or background, can thus vary accordingly, and is generally higher on the PEI interface than on the PSS and on the other modified rGO and Au surfaces.

To widen the concept of using modified rGO SPR interfaces for the study of *E. coli* tropism, glycan-modified interfaces were in addition investigated. Stronger capture densities of UTI89 and att25 are expected on mannose- or lactose-modified interfaces respectively (Table 2). Figure 7 shows a rather different SPR signature for both pathogenic strains. An interesting behavior is observed in the case of UTI89 (Figure 7A). After an increase in the SPR angle for the first 15 min, the SPR signal declines, giving *E. coli* UTI89 a specific SPR signature. This decline is believed to be a consequence of the noncovalently linked mannose to the Au/rGO SPR interface. Once in contact with the mannose-surface, UTI89 integrates mannose into its pocket and detaches it from the surface. Confocal microscope images recorded on mannose-terminated Au/rGO SPR interface after 15 and 80 min confirm this hypothesis (Figure 7C), where a rather different bacterial density can be visualized.

On the lactose-modified rGO, binding of the *E. coli* strain att25, specific to *N*-acetylglucosamine, a comparable result was obtained in the sense that the bacteria disintegrate the SPR interface (Figure 7D), resulting in an overall negative shift of the SPR angle (Figure 7E). Disintegration appears very rapidly with this adhesin, possibly due to the powerfull $\pi-\pi$ stacking of the lactose molecule with tryptophane (Trp) 108 and phenylalanine (Phe) 106 (Figure 3C). The other strains had a comparable, basal level of bacterial adhesion on the lactose-modified interface. The overall level of SPR change is also comparable to the other interfaces (Figure 5).

4. CONCLUSION

We have developed in this work a novel experimental concept for the investigation of pathogen tropism in an easy manner. The approach is based on the use of electrophoretically deposited reduced graphene oxide films onto gold SPR chips with subsequent chemical modification of the rGO with differently charged ligands such as positively charged polyethyleneimine (PEI) and negatively charged poly(sodium 4-styrenesulfonate) (PSS) as well as with glycans such as mannose or lactose. The summary of adhesion results reported in Figure 5A suggests that it is difficult to pinpoint the observed different interactions towards charge discrimination alone. However, it could be concluded that electrostatic interactions seem to be of higher importance than $\pi-\pi$ stacking interactions and that local charge variations close to the binding pockets of the bacteria seem to determine bacteria affinity. Chemically based affinity effects have to be considered in addition. Glycan interfaces show indeed specific binding events with sugar-specific *E. coli* strains such as UTI89 and att25. In the case of PSS and PEI modified Au/rGO SPR interface, a detection limit of ≈10^2 cfu/mL was achieved for *E. coli* 107/86 and UTI89, respectively. The advantage of such an approach is thus multiple: in contrast to bacteria sensing with bacteriophage where the size of the phage has an important implication on the proportion of the target bacteria which can be probed by the evanescent field of the SPR,[22] the modified rGO SPR interfaces allow probing of the entire bacteria without any constrain. The integration of affinity targets for different *E. coli* strains can be easily achieved through non-covalent interactions between the rGO matrix and various organic ligands. The strategy is thus adaptable to any other bacteria and more specifically if one is interested in examining bacterial affinities to molecules on a surface and quantitative detection of pathogen in solution. It should be possible to design novel experiments based on simplified model systems to answer many fundamental questions using this technique combining a plasmonic read out and graphene-based surface functionalization.

AUTHOR INFORMATION

Corresponding Authors

*E-mail: Sabine.Szunerits@iri.univ-lille1.fr.

*E-mail: Julie.Bouckaert@univ-lille1.fr.

Notes

The authors declare no competing financial interest.

ACKNOWLEDGMENTS

R.B. and S.S. gratefully acknowledge financial support from the Centre National de la Recherche Scientifique (CNRS), the University Lille 1 and the Nord Pas de Calais region. S.S thanks the Institut Universitaire de France (IUF) for financial support. P.S. acknowledges the financial support by the European Commission through RTN-project MATCON (Contract 238201). J.B. and N.Y. thank the CNRS and the French Agence National de la Recherche for grant ANR-12-BSV5-0016-01.

REFERENCES

(1) Viazis, S.; Diez-Gonzalez. *Adv. Agron.* **2011**, *111*, 1−50.

(2) Sokurenko, E. V.; Chesnokova, V.; Dykhuizen, D. E.; Ofek, I.; Wu, X.-R.; Krogelt, K. A.; Struve, C.; Schembri, M. A.; Hasty, D. L. *Proc. Natl. Acad. Sci. U.S.A.* **1998**, *95*, 8922.

(3) Chen, S. L.; Hung, C. S.; Pinkner, J. S.; Walker, J. N.; Cusumano, C. K.; Li, Z.; Bouckaert, J.; Gordon, J. I.; Hultgren, S. J. *Proc. Nat. Acad. Sci. U.S.A.* **2009**, *106*, 22439.

(4) Londardi, E.; Moonens, K.; Buts, L.; de Boer, A. R.; Olsson, J. D. M.; Weiss, M. S.; Fabre, E.; Guérardel, Y.; Deelder, A. M.; Oscarson, S.; Wuhrer, M.; Bouckaert, J. *Biology* **2013**, *2*, 894.

(5) Nishiyama, M.; Ishikawa, T.; Rechsteiner, H.; Glockshuber, R. *Science* **2008**, *320*, 376.

(6) Bouckaert, J.; Mackenzie, J.; de Paz, J. L.; Chipwaza, B.; Choudhury, D.; Zavialov, A.; Mannerstedt, K.; Anderson, J.; Pierard, D.; Wyns, L.; Seeberger, P. H.; Oscarson, S.; De Greve, H.; Knight, S. D. *Mol. Microbiol.* **2006**, *61*, 1556.

(7) Hung, C. S.; Bouckaert, J.; Hung, D.; Pinkner, J. S.; N., W. J.; Widberg, C.; DeFusco, A.; Gale Auguste, C.; Strouse, R.; Langermann, S.; Waksman, G.; Hultgren, S. J. *Mol. Microbiol.* **2002**, *44*, 903.
(8) Wellens, A.; Garofalo, C.; Nguyen, H.; Van Gerven, N.; Slättegård, R.; Hernalsteens, J. P.; Wyns, L.; Oscarson, S.; De Greve, H.; Hultgren, S. J.; Bouckaert, J. *PloS One* **2008**, *3* (4), e2040.
(9) Durka, M.; Buffet, K.; Iehl, J.; Holler, M.; Nierengarten, J.-F.; Taganna, J.; Bouckaert, J.; Vincent, S. P. *Chem. Commun.* **2011**, *47*, 1321.
(10) Barras, A.; Martin, F. A.; Bande, O.; Baumann, J. S.; Ghigo, J.-M.; Boukherroub, R.; Beloin, C.; Siriwardena, A.; Szunerits, S. *Nanoscale* **2013**, *5*, 2307.
(11) Lazcka, O.; Del Campo, F. J.; Munoz, F. X. *Biosens. Bioelectron.* **2007**, *22*, 1205.
(12) Belgrade, P.; Benett, W.; Hadley, D.; Richards, J.; Stratton, P.; Mariella, R.; Milanovich, F. *Science* **1999**, *284*, 449.
(13) Li, Y.; Cu, Y. T. H.; Luo, D. *Nat. Biotechnol.* **2005**, *23*, 885.
(14) Yang, L.; Li, Y.; Erf, G. F. *Anal. Chem.* **2004**, *76*, 1107.
(15) Guo, X.; Kulkarin, A.; Doepke, A.; Hlsall, H. B.; Iyer, S.; Heinemann, W. R. *Anal. Chem.* **2012**, *84*, 241.
(16) Wang, Y.; Ye, Z.; Ying, Y. *Sensors* **2012**, *12*, 3449.
(17) Yang, L.; Bashir, R. *Biotechnol. Adv.* **2008**, *26*, 135.
(18) Mannoor, M. S.; Tap, H.; Clyton, J. D.; Sengupta, A.; Kaplan, D. L.; Naik, R. R.; Verma, N.; Omenetto, F. G.; McAlpine, M. C. *Nat. Commun.* **2012**, *3*, 763.
(19) Maalouf, R.; Fournier-Wirth, C.; Coste-J.; Chebib, H.; Saikali, Y.; Vittori, O.; Errachid, A.; Cloarec, J.-P.; Martelet, C.; Jaffrezic-Renault, N. *Anal. Chem.* **2007**, *79*, 4879.
(20) Wan, Y.; Lin, Z.; Zhang, D. W.; Wang, Y.; Hou, B. *Biosens. Bioelectron.* **2011**, *26*, 1959.
(21) Yang, L. J.; Li, Y. B. *Biosens. Bioelectron.* **2005**, *20*, 1407.
(22) Oh, B.-K.; Lee, W. Y.; Chun, B. S.; Bae, Y. M.; Lee, W. H.; Choi, J.-W. *Biosens. Bioelectron.* **2005**, *20*, 1847.
(23) Gamella, M.; Campuzano, S.; Parrado, C.; Reviejo, A. J.; Pingarrón, J. M. *Talanta* **2009**, *78*, 1303.
(24) Mannoor, M. S.; Zhang, S.; Link, A. J.; McAlpine, M. C. *Proc. Natl. Acad. Sci. U.S.A.* **2010**, *107*, 19207.
(25) Tawill, N.; Sacher, E.; Mandeville, R.; Meunier, M. *Biosens. Bioelectron.* **2012**, *37*, 24.
(26) Singh, A.; Glass, N.; Tolba, M.; Brovoko, L.; Griffiths, M.; Evoy, S. *Biosens. Bioelectron.* **2009**, *24*, 3645.
(27) Wu, M. C.; Deokar, A. R.; Lao, J.-H.; Shih, P.-Y.; Ling, Y.-C. *ACSNano* **2013**, *7*, 1281.
(28) Das, M. R.; Sarma, R. K.; Borah, S. C.; Kumri, R.; Saikia, R.; Deshmukh, A. B.; Shelke, M. V.; Sengupta, P.; Szunerits, S.; Boukherroub, R. *Colloids Surf., B* **2012**, *105*, 128.
(29) Dreyer, D. R.; Park, S.-M.; Bielawski, C. W.; Ruoff, R. S. *Chem. Soc. Rev.* **2010**, *39*, 228.
(30) Szunerits, S.; Maalouli, N.; Wijaya, E.; Vilcot, J.-P.; Boukherroub, R. *Anal. Bioanal. Chem.* **2013**, *405*, 1435−1443.
(31) Subramanian, P.; Lesniewski, A.; Kaminska, I.; Vlandas, A.; Vasilescu, A.; Niedziolka-Jonsson, J.; Pichonat, E.; Happy, H.; Boukherroub, R.; Szunerits, S. *Biosens. Bioelectron.* **2013**, *50*, 239−243.
(32) Salihoglu, O.; Balci, O.; Kocabas, C. *Appl. Phys. Lett.* **2011**, *100*, 213110.
(33) Wu, M.; Kempaiah, R.; Jimmy Hunag, P.-J.; Maheshwari, V.; Liu, J. *Langmuir* **2011**, *27*, 2731.
(34) Nielsen, N. O.; Clugston, R. E. *Ann. N. Y. Acad. Sci.* **1971**, *176*, 176.
(35) Hummers, W. S.; Offerman, J. R. E. *J. Am. Chem. Soc.* **1958**, *80*, 1339.
(36) Das, M. R.; Sarma, R. K.; Saikia, R.; Kale, V. S.; Shelke, M. V.; Sengupta, P. *Colloid Surf. B: Biointerfaces* **2011**, *83*, 16.
(37) Wink, T.; Van Zuilen, S. J.; Bult, A.; Van Bennekom, W. P. *Anal. Chem.* **1998**, *70*, 827.
(38) Kooyman, R. P. H.; Lenferink, A. T. M.; Eenik, R. G.; Greve, J. *Anal. Chem.* **1991**, *63*, 83.
(39) Szunerits, S.; Maalouli, N.; Wijaya, E.; Vilcot, J. P.; Boukherroub, R. *Anal. Bioanal. Chem.* **2013**, *405*, 1435.
(40) Kaminska, I.; Barras, A.; Coffinier, Y.; Lisowski, W.; Niedziolka-Jonsson, J.; Woisel, P.; Lyskawa, J.; Opallo, M.; Siriwardena, A.; Boukherroub, R.; Szunerits, S. *ACS Appl. Mater. Interfaces* **2012**, *4*, 5386.
(41) Busscher, H. J.; van der Mei, H. *PLOS Phathogens* **2012**, *8*, e1002440.
(42) Terada, A.; Yuasa, A.; Kushimoto, T.; Tsuneda, S.; Katakai, A.; Tamada, M. *Microbiol.* **2006**, *152*, 3575.
(43) Arya, S. K.; Singh, A.; Naidoo, R.; Wu, P.; McDermott, M. T.; Evoy, S. *Analyst* **2011**, *136*, 486.
(44) Oh, B.-K.; Kim, Y. K.; Lee, W. H.; Bae, Y. M.; Lee, W. H.; Choi, J. W. *Biosens. Bioelectron.* **2003**, *18*, 605.
(45) Wilson, M.L.; Gaido, L. *Clin. Infect. Dis.* **2004**, *38*, 1150.